Photocatalysis

International Edition: DOI: 10.1002/anie.201411096
German Edition: DOI: 10.1002/ange.201411096

Graphene-Based Photocatalysts for Solar-Fuel Generation

*Quanjun Xiang, Bei Cheng, and Jiaguo Yu**

Keywords:
CO_2 reduction · graphene · hydrogen production · photocatalysis · solar fuel

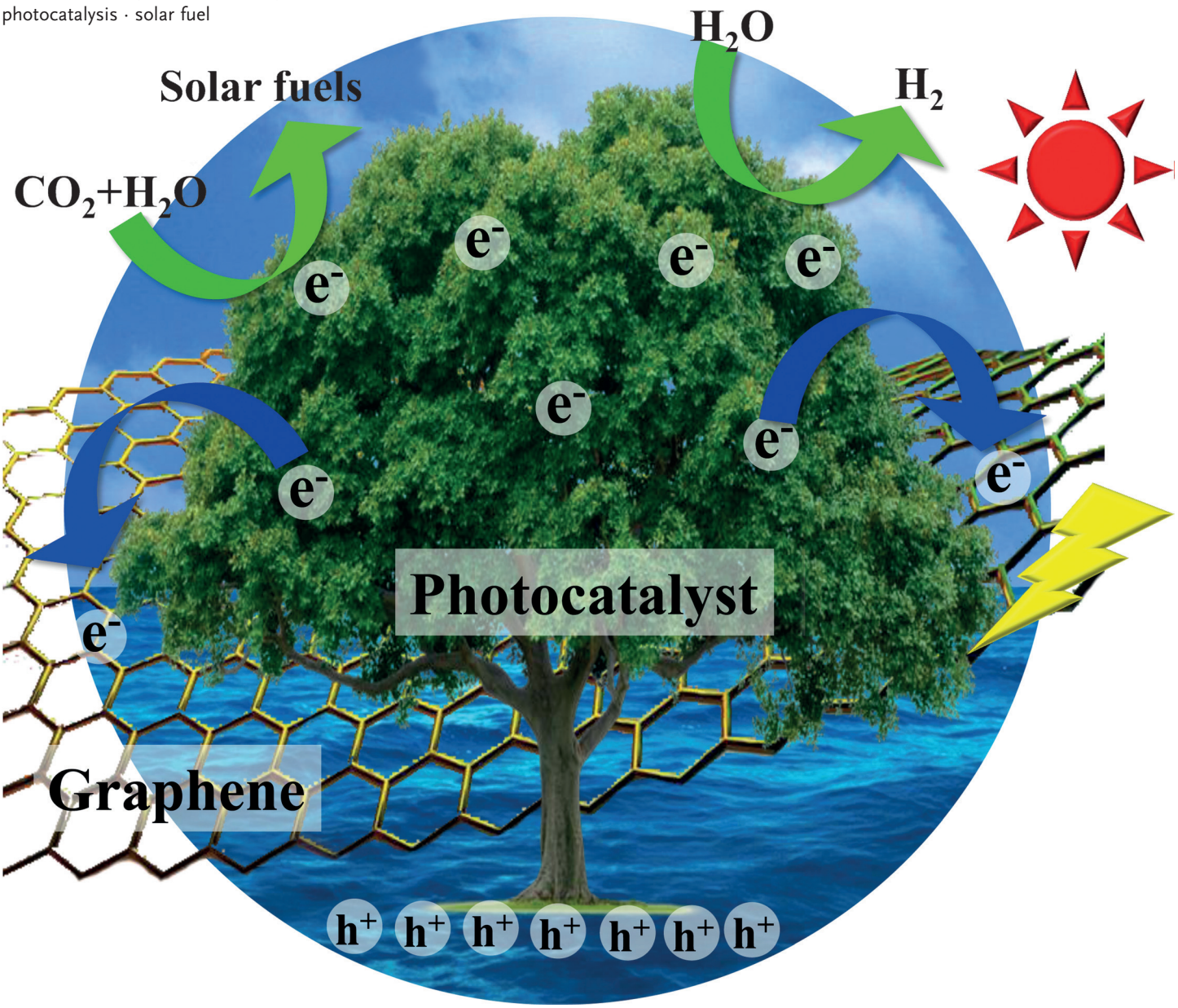

The production of solar fuel through photocatalytic water splitting and CO_2 reduction using photocatalysts has attracted considerable attention owing to the global energy shortage and growing environmental problems. During the past few years, many studies have demonstrated that graphene can markedly enhance the efficiency of photocatalysts for solar-fuel generation because of its unique 2D conjugated structure and electronic properties. Herein we summarize the recent advances in the application of graphene-based photocatalysts for solar-fuel production, including CO_2 reduction to hydrocarbon fuel and water splitting to H_2. A brief overview of the fundamental principles for splitting of water and reduction of CO_2 is given. The different roles of graphene in these graphene-based photocatalysts for improving photocatalytic performance are discussed. Finally, the perspectives on the challenges and opportunities for future research in this promising area are also presented.

From the Contents

1. Introduction

Global energy shortage and growing environmental pollution, as well as global climate change are considered to be among the biggest challenges of this century that humanity faces. Solar fuel is regarded as a potentially significant alternative for sustainable and clean energy in future. What is termed solar fuel is often in the form of converting solar energy into energy stored in chemical bonds. The production of solar fuel has attracted a lot of attention because of its potential for solving the global energy and the related environmental issues.[1] Solar energy is the most abundant and renewable source of clean energy. Therefore, it is desirable to develop artificial photosynthetic systems that can produce chemical fuels by solar-energy conversion. Semiconductor photocatalytic technology, used to directly convert solar energy into chemical energy, has been recognized as one of the most widely studied solar-fuel strategies for the photocatalytic splitting of water into H_2 and O_2, and the photocatalytic reduction of CO_2 into hydrocarbon fuels, because semiconductors are cost-effective, simple, and convenient, and have huge potential for further development.[2–7]

The photoelectrocatalytic splitting of water on TiO_2 electrodes and the photoelectrocatalytic reduction of CO_2 in aqueous suspensions of semiconductor powders were first reported by Fujishima and Honda[2] in 1972 and Inoue et al.[3] in 1979, respectively. Since then, the principles of photoelectrocatalytic H_2 production and CO_2 reduction have been extended, and photocatalytic H_2 production and CO_2 reduction have been extensively studied. In principle, the basic process of photocatalytic water splitting and CO_2 reduction can be summarized into three steps: 1) generation of photogenerated charge carriers (electron–hole pairs) by a band-gap excitation, 2) separation and transportation of the charge carriers, 3) reduction of water or carbon dioxide by the photogenerated electrons. As shown in Figure 1, when a semiconductor is excited by a photon with energy equivalent to or higher than the band gap, electrons in the conduction band and positive holes in the valence band are generated. Thus, the photogenerated electrons and holes may migrate to the surface of the semiconductor, and then, respectively, reduce or oxidize the reactants adsorbed on the semiconductor surface. In this case, such reduction reactions in the photocatalytic system can catalyze the production of H_2 from water splitting and induce the reduction of CO_2 to hydrocarbon fuel. However, for the production of solar fuel in such a photo-

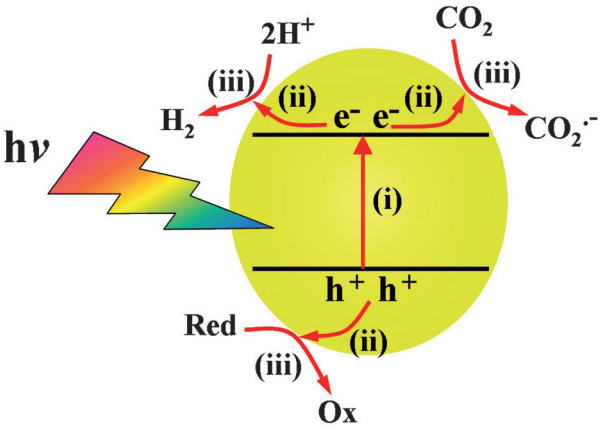

Figure 1. Schematic illustration of basic mechanism of hydrogen production and CO_2 reduction with a semiconductor photocatalyst.

[*] Dr. Q. Xiang
College of Resources and Environment, Huazhong Agricultural University, Wuhan 430070 (P.R. China)
Prof. B. Cheng, Prof. J. Yu
State Key Laboratory of Advanced Technology for Materials Synthesis and Processing, Wuhan University of Technology
Wuhan 430070 (P.R. China)
Prof. J. Yu
Department of Physics, Faculty of Science
King Abdulaziz University
Jeddah 21589 (Saudi Arabia)
E-mail: jiaguoyu@yahoo.com
Homepage: http://www.researcherid.com/rid/G-4317-2010

catalytic system, the positions of the valence band and conduction band of semiconductor photocatalyst should both match the oxidation and reduction potentials of water splitting and CO_2 reduction. In fact, only a few semiconductors satisfy the above-mentioned requirements for the splitting of water and/or the reduction of CO_2 under solar-light irradiation.[1,6] As shown in Figure 2, the position of the conduction band edge should be more negative than that of the redox potential of H_2/H_2O or CO/CO_2 (or hydrocarbons/CO_2).[8–10] Meanwhile, the potential of the valance band edge should be more positive than the redox potential of O_2/H_2O. As in such case, semiconductor photocatalysis based on photogenerated charge carriers can produce H_2 from water splitting and induce the reduction of CO_2 to hydrocarbon fuels. Equations (1)–(8) illustrate the chemical reactions for solar-fuel generation at pH 7 in aqueous solution.

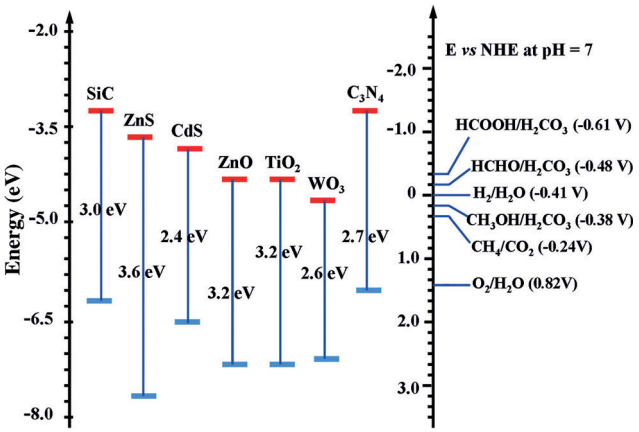

Figure 2. Band-edge positions of selected semiconductor photocatalysts relative to the energy levels of various redox couples at pH 7 in aqueous solution.

For the photocatalytic H_2 production, the reduction potential of water to hydrogen is −0.42 V versus the normal hydrogen electrode (NHE) at pH 7, and reduction of the protons to a H_2 molecule is a two-electron process. The photocatalytic reduction of CO_2 to hydrocarbon fuels is more challenging and a complicated photophysical and photochemical process. For example, the products in photocatalytic conversion of CO_2 may include HCOOH, HCHO, CH_3OH, CO, H_2, and CH_4. Thus, the products in photocatalytic CO_2 reduction are selective and are dependent on many factors, such as reaction kinetics, redox potentials of photoinduced carriers, morphology, and the surface properties of the photocatalyst and the loaded co-catalysts.[9–14] It is believed that Pt and Au as co-catalysts can selectively reduce CO_2 into CH_4 products. Recently, it has been reported that there are two different morphologies of Cu_2O photocatalysts which result in dramatic differences in product selectivity.[14] In addition, the selectivity of the process is very difficult to control. From a thermodynamic point of view, the production of CH_4 by photocatalytic reduction of CO_2 is relatively easy because the reduction potential for CH_4/CO_2 is −0.24 V versus NHE at pH 7, however, the reaction of eight electrons with eight protons and CO_2 is extremely difficult from a kinetics point of view. In addition, the production of methanol and formaldehyde is a 4–6-electron process and is also kinetically difficult, while the reduction of CO_2 to CO or formic acid has a very negative chemical potential (−0.53 or −0.61 V vs. NHE at pH 7). Nevertheless, the thermodynamic reduction potential and the kinetic electron reaction both need to be taken into account for photocatalytic H_2 production and CO_2 reduction.

Reaction		E^o (V vs NHE)
$CO_2 + 2e^- \rightarrow {\bullet}CO_2^-$	(1)	−1.90
$CO_2 + 2H^+ + 2e^- \rightarrow HCOOH$	(2)	−0.61
$CO_2 + 2H^+ + 2e^- \rightarrow CO + H_2O$	(3)	−0.53
$CO_2 + 4H^+ + 4e^- \rightarrow HCHO + H_2O$	(4)	−0.48
$CO_2 + 6H^+ + 6e^- \rightarrow CH_3OH + H_2O$	(5)	−0.38
$CO_2 + 8H^+ + 8e^- \rightarrow CH_4 + 2H_2O$	(6)	−0.24
$2H_2O + 4H^+ \rightarrow O_2 + 4H^+$	(7)	+0.81
$2H^+ + 2e^- \rightarrow H_2$	(8)	−0.42

Although photocatalytic H_2 production and CO_2 reduction show great potential for further development, at present one of the greatest drawbacks is the low conversion efficiency. For photocatalytic H_2 production, a maximum theoretical efficiency for the conversion of solar energy into hydrogen fuel is 31% for a single photocatalyst material. During the past few decades, great progress has been made and yet the energy conversion efficiency for solar hydrogen production is below 5%.[8] Compared to the two-electron H_2 production,

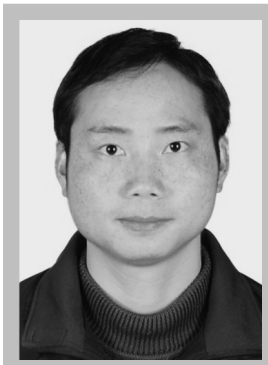

Quanjun Xiang received his BS in 2007 at Henan Polytechnic University. He obtained his PhD in Materials Chemistry & Physics in 2012 from Wuhan University of Technology under the supervision of Prof. Jiaguo Yu. He was a post-doctoral fellow at the City University of Hong Kong from 2013 to 2015. He is now an Associate Professor at Huazhong Agricultural University. His current research interests focus on design and synthesis of graphene-based photocatalysts for energy and environmental applications.

Bei Cheng received her BS and MS in Materials Science from Tongji University, her PhD in Materials Science in 2006 from Wuhan University of Technology under the supervision of Prof. Xiujian Zhao. In 2010, she became a Professor of Wuhan University of Technology. Her research interests include semiconductor photocatalytic materials, photocatalytic hydrogen production, dye-sensitized solar cells.

photocatalytic CO_2 reduction is comparatively more complex and the achieved efficiency of solar to carbon-based fuel is only 1 % for a single semiconductor material because most of the chemical reactions of the CO_2 reduction require 4–8 electrons and a more-negative reduction potential. Taking into consideration the basic chemical reactions for photocatalytic H_2 production and CO_2 reduction, an efficient charge separation is essential for photocatalytic solar-fuel generation. The enhancement of photocatalytic activity is ascribed to suppressing the recombination of the photogenerated electrons and holes. Several strategies to aid the charge separation and migration have been proposed, such as the addition of a noble metal and the utilization of a highly electrical conductive material.[15] In particular, many studies have demonstrated that the use of graphene in photocatalysis can significantly improve the performance of the photocatalysts.[16–22] As shown in Figure 3, because of its high work function and good conductivity, graphene can act as an electron acceptor/transporter to induce electrons transfer from the conduction band of semiconductors to graphene, leading to an efficient charge separation. In addition, graphene could also serve as a co-catalyst to catalyze H_2 production and CO_2 reduction because the reduction potential of graphene is more negative than the reduction potential of water to hydrogen and of CO_2 to hydrocarbon fuels. In principle, the intrinsic structural and electronic properties of graphene can be tuned by heteroatom doping or by an electrostatic field. Therefore, the excited electrons on the conduction band of the semiconductor may migrate to a carbon material to drive the chemical reactions of H_2 production and CO_2 reduction.

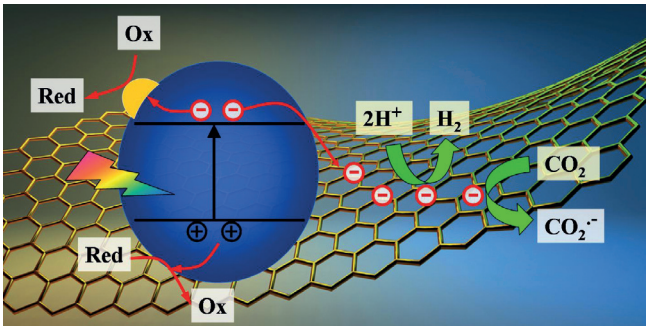

Figure 3. Charge transfer and separation in graphene-based semiconductor photocatalysts for photocatalytic hydrogen production and CO_2 reduction.

Graphene, as a new type of carbon nanomaterial, has attracted considerable attention since its discovery in 2004,[23] owing to its mechanical, thermal, optical, and electrical properties. In general, graphene is considered to be a zero band-gap semiconductor with a symmetric band structure. The unique band structure gives graphene outstanding conductivity and electron mobility properties. Considering the unique two-dimensional structure with its high specific surface area and favorable electronic properties, make conductive graphene an ideal support for constructing a new type of graphene-based photocatalysts with enhanced photocatalytic performance.[24–26] Graphene can serve as a high electrical conductivity material to facilitate the charge separation and migration. Especially, the use of graphene could make the multi-electron reduction process of CO_2 more efficient and through its unique electron-collecting and -transfer capabilities promote the selective production of specific fuels in photocatalytic CO_2 reduction. In addition, graphene can function as a co-catalyst replacing noble metals to drive the redox reaction for solar fuel generation. As well as graphene, graphene oxide and its analoguescan act as a small-band-gap semiconductors after adjusting their degree of oxidation, which may make them aromatic macromolecule photoabsorbers to extend the absorption wavelength of light, and as potential candidates of non-metal semiconductor photocatalysts. For instance, it has been reported that a graphene oxide semiconductor photocatalyst could steadily catalyze H_2 generation from a 20 vol % aqueous methanol solution.[27] Research on graphene-enhanced photocatalysis is advancing fast.[28–35] Much research work has been attempted to design and prepare novel graphene-based semiconductor photocatalysts and explore their potential applications in environmental processes and energy conversion, including photocatalytic pollutant degradation,[36–38] photocatalytic disinfection,[39] photocatalytic hydrogen generation,[40] and photocatalytic reduction of CO_2.[41] For example, Zhang et al.[18] produced graphene/P25 TiO_2 composites by a hydrothermal method. The composites exhibited a significantly enhanced photocatalytic degradation of methylene blue in aqueous solutions. Ng et al.[42] demonstrated the improved photo-electrochemical efficiency of the graphene oxide/$BiVO_4$ composite photocatalyst by one order of magnitude. Especially, in recent years, particular attention has been paid to photocatalytic H_2 production and CO_2 reduction by graphene-based photocatalysts, which is the focus of this Review.

Herein, we focus upon the use of graphene-based photocatalysts for the production of solar fuel, including photocatalytic splitting of water to H_2 and photocatalytic reduction of CO_2 to hydrocarbon fuels. Notably, the application of graphene-based photocatalysts in the photocatalytic reduction of CO_2 to hydrocarbon fuels has not been fully covered by the previous Reviews.[22,28–34] Herein we concisely summarize the recent advances in these applications of graphene-based photocatalysts. The different roles of graphene in

Jiaguo Yu received his BS and MS in chemistry from Central China Normal University and Xi'an Jiaotong University, respectively, and his PhD in Materials Science in 2000 from Wuhan University of Technology under the supervision of Prof. Xiujian Zhao. In 2000, he became a Professor at Wuhan University of Technology. He was a postdoctoral fellow at the Chinese University of Hong Kong (2001–2004), a visiting scientist at University of Bristol (2005–2006), and University of Texas at Austin (2007–2008). His research interests include semiconductor photocatalysis, photocatalytic hydrogen production, CO_2 reduction to hydrocarbon fuels.

improving the photocatalytic performance are summarized, including the role of graphene as electron acceptor and transporter, co-catalyst, photosensitizer, coupler, and photocatalyst. The existing challenges for future development of graphene-based photocatalysts for solar-fuel generation are also discussed. We hope that this Review can further promote the design and fabrication of graphene-based photocatalysts with better performances based on the outstanding structural and electronic properties of graphene and expand their functional applications in photocatalytic H_2 production and CO_2 reduction.

2. Photocatalyitc Reduction of CO_2

Global warming and energy shortage are two critical issues this century. CO_2 is the most abundant greenhouse gas in the atmosphere and plays an important role in global warming. In the past several decades, the rising concentration of atmospheric CO_2 resulting from the consumption of fossil fuels results in the global warming.[9,43,44] To date, several methods such as absorption, bioconversion, photocatalytic reduction, and capture and transfer, have been developed for reducing the amount of atmospheric CO_2.[8,45,46] Photocatalytic reduction of CO_2 has attracted considerable attention in recent years because this method can convert CO_2 into hydrocarbon fuels, such as CH_4 and CH_3OH. Since the first report by Inoue and co-workers[3] on the photoelectrocatalytic reduction of CO_2 to formaldehyde and methanol, various metal oxides, metal sulfides, and oxynitride semiconductor photocatalysts have been developed for the photocatalytic reduction of CO_2 to fuels.[12] Studies of these systems usually focus on the half-reactions of the CO_2 reduction, and an artificial electron donor needs to be used in the photocatalytic CO_2 reduction reaction, which is a great drawback in solar-fuel applications. In such cases, water is an ideal electron donor in future studies. In addition, practical applications of photocatalytic reduction of CO_2 are limited because of the low fuel-conversion efficiency caused by the rapid recombination of photogenerated electrons and holes within photocatalysts. Therefore, increasing the efficient utilization of solar energy and decreasing the recombination of photogenerated charge carriers and/or enhancing the transfer of photogenerated electrons are very desirable to enhance the efficiency of photocatalytic CO_2 reduction.

2.1. Graphene-Based Photocatalysts

Recently, graphene has demonstrated its promising function as an efficient electron acceptor and transporter that enhances the transfer of photogenerated electron and prolongs the lifetime of photogenerated charge carriers. Thus, graphene-based semiconductor photocatalysts have been widely used in the photocatalytic reduction of CO_2.[43–56] For example, Liang et al.[49] reported the solvent-exfoliated graphene/P25 TiO_2 nanocomposite thin film as a highly efficient photocatalyst for the visible-light photocatalytic reduction of CO_2. The optimized graphene–TiO_2 nanocomposite film displayed a sevenfold improvement in photocatalytic reduction of CO_2 compared to pure TiO_2 under visible-light irradiation. This improvement was due to the low defect density in solvent-exfoliated graphene, which improved the electrical mobility and facilitated the transfer of the photoexcited electrons to reactive sites. In particular, the incorporation of graphene into P25 TiO_2 extends the optical absorption of TiO_2 to longer wavelengths, leading to photocatalytic activity in the visible-light range. This could be attributed to the formation of Ti-O–C bonds in graphene/P25 nanocomposites. The carbonate structural fragments of graphene with unpaired π electrons can bond with the titanium atoms of TiO_2, the chemical bonding between TiO_2 and graphene can extend the light absorption range. Further studies are still needed to develop visible-light responsive photocatalysts based on carbonate structural fragments bound to titanium. This important work is just part of the research in the area of graphene-based semiconductor photocatalysts for visible-light photocatalytic CO_2 reduction. Subsequently, Liang et al.[50] investigated the influence of carbon nanomaterial dimensionality on the photocatalytic reduction of CO_2 by comparing the photocatalytic performance of carbon nanotube/titania nanosheet and graphene/titania nanosheet composites. As a result of the two-dimensional (2D) nature of graphene, the 2D–2D graphene/titania nanosheet composites exhibited a more intimate interfacial contact and superior optoelectronic coupling with titania nanosheets, leading to an enhanced photocatalytic activity of CO_2 reduction as compared to 1D–2D carbon nanotube/titania nanosheet under ultraviolet light illumination. The above studies have opened a new way for the utilization of 2D graphene-sheet-based photocatalysts in the reduction of CO_2.

In general, the interface between photocatalysts and graphene in the graphene-based composite photocatalysts strongly affects the photocatalytic activity. In particular, it is well documented that a large contact area and strong interaction between the components can promote the transfer of electrons in the photocatalytic reaction and improve the performance.[31,57–61] Tu et al.[51] have developed a hollow-sphere composite consisting of titania ($Ti_{0.91}O_2$) nanosheets and graphene oxide (GO) nanosheets with a molecular-scale 2D contact between $Ti_{0.91}O_2$ and GO. The molecular-scale 2D contact and the hollow structure in this composite facilitate the charge separation and enhance the lifetime of the charge carriers and therefore improve the photocatalytic efficiency. Surprisingly, this graphene/$Ti_{0.91}O_2$ nanocomposite shows a nine-times enhancement of the photocatalytic activity compared to commercial P25 TiO_2 for the photocatalytic conversion of CO_2 into CO and CH_4. In the subsequent work, another 2D sandwich-like graphene/TiO_2 hybrid nanosheet composite was also synthesized by an in situ reduction-hydrolysis method in a binary ethylenediamine (En)/H_2O solvent.[52] As shown in Figure 4 a,b, a large number of TiO_2 nanoparticles are uniformly dispersed and tightly packed on the surface of graphene sheets to form a 2D sandwich-like structure. This close neighborhood of TiO_2 and graphene in the hybrid can favor the transfer of photogenerated electrons from TiO_2 to graphene sheets, and thus facilitate the charge separation efficiency. Furthermore, the presence of abundant

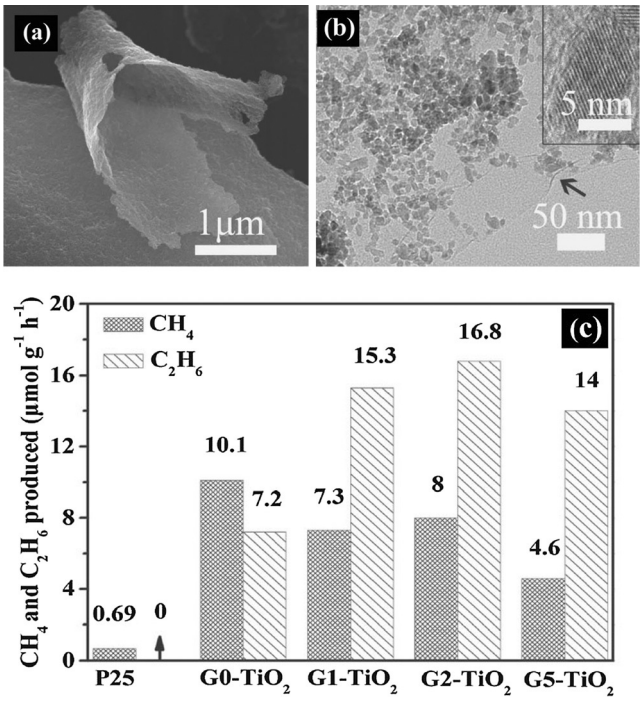

Figure 4. a) FESEM and b) TEM images of graphene/TiO_2 hybrid nanosheet composites; c) Photocatalytic activity of G*x*/TiO_2 ($x = 0, 1, 2, 5$) samples and P25. Reprinted with permission from Ref. [52]. Copyright 2013, Wiley-VCH.

Ti^{3+} sites on the surface of TiO_2 creates a low-coordinated oxygen species, which leads to an increase of the number of basic sites in TiO_2. In the CO_2 reduction, it is the basic TiO_2 sites which give rise to the photocatalytic product selectivity towards CH_4 and C_2H_6. Therefore, it is not surprising that the graphene/TiO_2 hybrid nanosheets with abundant Ti^{3+} sites in TiO_2 showed enhanced photocatalytic performance for the reduction of CO_2 into CH_4 and C_2H_6 compared to commercial P25 and blank TiO_2. In addition, the effect of the graphene content in the hybrid nanosheets on the conversion efficiency of photocatalytic CO_2 reduction into hydrocarbon fuel was also studied. As shown in Figure 4c, the graphene content has a great effect on the photocatalytic activity. With increasing graphene content, the production rate of CH_4 slowly decreases but the production rate of C_2H_6 noticeably increases. This change is attributed to two factors: 1) The lower conversion rate of CH_4 for graphene/TiO_2 (G-TiO_2) nanocomposites is because methyl radicals ($\cdot CH_3$) are intermediates and can be absorbed on the surface of graphene by π-conjugation. 2) The enhanced C_2H_6 production rate is because of the chemical bond interactions in the G-TiO_2 nanocomposites which favor the transfer of excited-state electrons to the graphene surface where they can react with CO_2. However, there is an optimized graphene content which gives the greatest overall production rate of CH_4 and C_2H_6 in the photocatalytic CO_2 conversion.

Apart from graphene/TiO_2 composites, composites of graphene and other photocatalysts, such as graphene/CdS,[41] graphene/ZnO,[53] graphene/WO_3,[54] and graphene/NiO_x/Ta_2O_5[55] have also been reported as promising for the catalytic conversion of CO_2 into solar fuel. For example, Yu and co-workers[41] reported highly active reduced graphene oxide (RGO)/CdS nanorod composite photocatalysts for the visible-light photocatalytic reduction of CO_2 to CH_4. The RGO acts as an electron acceptor and transporter to facilitate the separation of photogenerated charge carriers, and enhances the adsorption and activation of CO_2 molecules and subsequently accelerates the photocatalytic reduction of CO_2 to CH_4. It demonstrates for the first time that RGO can be an effective co-catalyst for enhancing the photocatalytic reduction of CO_2 to CH_4. RGO also acted as an effective co-catalyst in ZnO/RGO nanocomposites,[53] giving a 75% improvement in efficiency for the photocatalytic reduction of CO_2. This improvement is because RGO acts as the reducing sites and reacts with the absorbed CO_2. In spite of the recent progress in the development of graphene as a co-catalyst in photocatalytic CO_2 reduction,[41,53] much effort needs to be further made in developing the utilization of graphene sheets as a co-catalyst for replacing noble metals in this process.

Another approach that has been proposed for graphene-based photocatalysts for photocatalytic CO_2 reduction is to shift the Fermi level and/or the conduction band potential of the semiconductor photocatalyst.[54,56] Wang et al.[54] reported graphene/WO_3 nanobelt composites as an efficient photocatalyst for catalytic reduction of CO_2 into CH_4. Significantly, they pointed out that, although the conduction band (CB) minimum of WO_3 is inherently limited for photocatalytic CO_2 reduction, graphene can elevate the conduction band of WO_3 in the composites. This change is due to the formation of strong covalent bonds between graphene and WO_3 by the hydrothermal treatment of graphene oxide and the precursor of WO_3. During the hydrothermal process, graphene oxide is reduced to graphene, while simultaneously, the WO_3 nanobelts are dispersed on the graphene sheets, leading to the covalent interactions between graphene and WO_3. Thus, the electronic interaction and the charge equilibration between graphene and WO_3 in the graphene/WO_3 composite can cause a negative shift of the Fermi level of the graphene/WO_3 composite under irradiation. The elevated CB minimum of the graphene/WO_3 composite is higher than the redox potential of CH_4/CO_2 and can cause the photocatalytic reduction of CO_2 to CH_4 under visible-light irradiation (see Figure 5). This work provides a new direction for tuning the photoreactivity of graphene-based photocatalysts for photocatalytic CO_2 reduction. Recently, a ternary graphene-modified/NiO_x/Ta_2O_5 composite photocatalyst has been synthesized for the photocatalytic reduction of CO_2 with H_2O.[55] The anisotropic multicomponent nanomaterials consisting of graphene, NiO_x, and Ta_2O_5 can facilitate the charge separation at different levels in the ternary nanocomposite. The excellent electron-collecting and -transferring capabilities of graphene promote the multi-electron reduction of CO_2, which leads to high yields of methanol and hydrogen in the photocatalytic reaction.

2.2. Graphene-Based Photoelectrocatalysts

Photoelectrocatalysis is another promising way to reduce CO_2 to chemical fuels. In contrast to photocatalytic CO_2

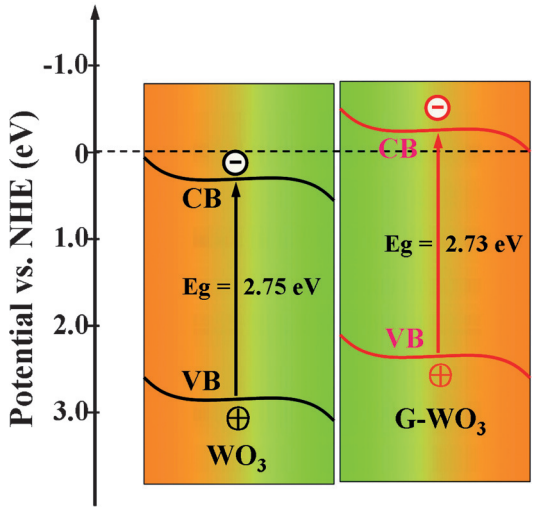

Figure 5. Energy-level diagram for pure WO_3 and graphene/WO_3 composite versus NHE (pH 7).

reduction, photoelectrocatalysis is carried out in a photoelectrochemical cell with an applied electrical bias. In such a system, the use of an electrical bias represents an additional energetic input and is undesirable for technological applications. However, the role of an electrical bias can increase the surface space charge layer and the magnitude of the electric fields, which can increase the lifetime of photogenerated charges, leading to higher photocatalytic efficiency.[8] For example, the use of Fe_2O_3 photoelectrodes in a photoelectrochemical cell results in the increase of charge carrier lifetime by a factor of 10^3 on the application of 400 mV anodic bias, which then improves the catalytic activity.[62] Recently, graphene-based catalytic materials were used as a photoelectrocatalyst in the reduction of CO_2.[63,64] For example, Cheng et al.[63] reported a photoelectrocatalytic reduction of CO_2 to chemical fuels using Pt-modified reduced graphene oxide and Pt-modified TiO_2 nanotubes as cathode and photoanode catalysts, respectively. As shown in Figure 6, the photoelectrocatalytic reactor system was separated into two physically distinct areas for water oxidation and CO_2 reduction. At the

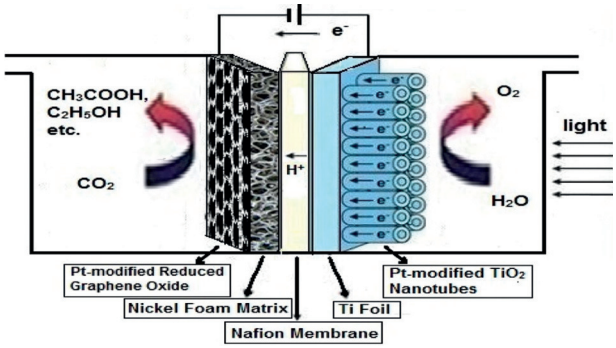

Figure 6. Schematic illustration of the photoelectrocatalytic reaction system using Pt-modified reduced graphene oxide as a cathode catalyst and Pt-modified TiO_2 nanotubes as a photoanode catalyst. Reprinted with permission from Ref. [63]. Copyright 2014, American Chemical Society.

anode of Pt-modified TiO_2 nanotubes, the electrolysis of water by the photogenerated holes leads to the formation of gaseous oxygen and hydrogen ions when the bias potential was applied. Meanwhile, the photogenerated electrons are driven to the cathode of Pt-modified reduced graphene oxide by a potentiostat causing the reduction of CO_2 to hydrocarbons. Owing to the high reactant adsorptivity and efficient charge transportation of graphene, the photocathode catalyst of Pt-modified reduced graphene oxide can convert CO_2 into chemical fuels efficiently. Recently, Tripkovic et al.[64] investigated the catalytic activity of the metal-functionalized porphyrin-like graphene for the electrochemical reduction of CO_2 and CO to methane or methanol. Notably, the photoelectrocatalytic reactions usually convert CO_2 into high-value liquid products, such as C_2H_5OH and CH_3COOH, which can be stored, transported, and used easily. In addition, the conversion efficiency of CO_2 photoelectrocatalytic reactions is relative high and stable in compared with that of the CO_2 photocatalytic reaction. However, the current conversion efficiency of the photoelectrocatalytic reduction of CO_2 is still low for industrial application. A further exploration of graphene-based catalytic materials is needed for developing high conversion-efficiency CO_2 photoelectrocatalytic reactions.

2.3. Graphene-Based Biocatalysts

Research on graphene-based photocatalysts for catalytic CO_2 reduction, usually employs photocatalysts that are metal oxide semiconductors or transition-metal complexes. However, owing to the small energy difference between the conduction band edges of metal oxide and the reduction potential of biocatalysts the graphene/metal oxide semiconductor composites were not suitable as a highly effective photocatalyst for photocatalyst/biocatalyst coupled systems.[65] Photocatalyst/biocatalyst coupled systems are also exploited for the production of solar fuels/chemicals by CO_2 reduction.[65,66] For instance, Yadav et al.[65] reported a new graphene-photocatalyst/enzyme coupled system for an efficient artificial photosynthetic production of formic acid from CO_2 conversion. The coupling of chemically converted graphene to a chromophore (a multianthraquinone-substituted porphyrin) gave a visible-light active photocatalyst and formate dehydrogenase served as an enzyme for the enzymatic conversion of CO_2 into formic acid. This novel graphene-based chromophore photocatalyst shows higher efficiency for the production of formic acid from CO_2 than other photocatalysts, such as $W_2Fe_4Ta_2O_{17}$ and multianthraquinone-substituted porphyrin. The enhancement is because the photoexcited electrons generated on the multianthraquinone-substituted porphyrin can be effectively transferred into the graphene in this system due to its extremely high carrier mobility. Subsequently, Yadav et al.[66] further demonstrated that graphene/BODIPY can be used as an efficient visible-light active photocatalyst in the photocatalytic/biocatalytic coupled system for the production of nicotinamide adenine dinucleotide (NADH) and formic acid from CO_2 conversion. It is suggested that the high NADH regeneration and the

exclusive formation of formic acid from CO_2 originates from the presence of highly efficient visible-light-harvesting BODIPY molecule and the large potential difference of BODIPY molecule and graphene, which enables the generation of photoexcited electrons and the efficient transfer of the electrons. Very recently, Han and co-workers[67] reported a composite photocatalyst consisting of graphene and porphyrin for the highly efficient conversion of CO_2 into CH_4 and C_2H_2 under visible-light irradiation. However, for such graphene-based biocatalysts, one clear drawback is that most of the organic molecules used in such catalysts are usually not stable under illumination in an aqueous dispersion because of the photoinduced intra- and intermolecular electron transfer in the organic molecules. In this regard, one of the most challenging tasks is the search for a stable and highly efficient organic molecule catalyst in graphene-based biocatalyst systems. Overall, the above studies provide a promising new direction to photocatalyst/biocatalyst coupled artificial photosynthesis systems using graphene-based materials. Nevertheless, the graphene-enhanced artificial photosynthesis process needed to be clarified and further exploited for solar fuels/chemicals production from CO_2 conversion.

2.4. Using Graphene Oxide Itself as a Photocatalyst

In addition to graphene-based composites, graphene oxide (GO) with additional oxygenated components was also found to be a promising photocatalyst for the catalytic CO_2 reduction to methanol. Hsu et al.[68] have reported that graphene oxides prepared by the modified Hummer's method exhibited a high photocatalytic conversion rate of CO_2 into methanol under simulated solar-light irradiation. They found that the synthesized GO samples with different optical band gaps exhibited a significant influence on the activity of photocatalytic CO_2 reduction to methanol (see Figure 7a). The GO-3 sample with wide band gap displayed the maximum methanol conversion rate and remained chemically stable during irradiation. In particular, the methanol conversion rate over the optimized GO-3 sample was six-fold higher than with pure commercial P25 TiO_2 under the same experimental conditions. This unusual activity for the photocatalytic CO_2 reduction on graphene oxides can be attributed to the fact that modified graphene oxides with additional oxygenated functional groups can be excited to generate electron–hole pairs under irradiation. The photogenerated electrons and holes can migrate to the surface of the graphene oxides and serve as the reduction and oxidation sites, respectively. These photogenerated electrons and holes have the appropriate reduction and oxidation potentials, to react with the adsorbed CO_2 and H_2O to produce methanol in a six-electron reaction (see Figure 7b). Moreover, the GO photocatalyst in this system is chemically stable during the photocatalytic process. Although the conversion efficiency of photocatalytic CO_2 reduction on GO photocatalysts is low and the modified process for the synthesis of GO photocatalysts is complicated, this study pioneers the new concept of low-cost GO photocatalysts for CO_2 reduction. The above work highlights the interesting application of graphene oxide itself as an efficient photocatalyst for catalytic CO_2 reduction to hydrocarbon fuels under solar illumination.

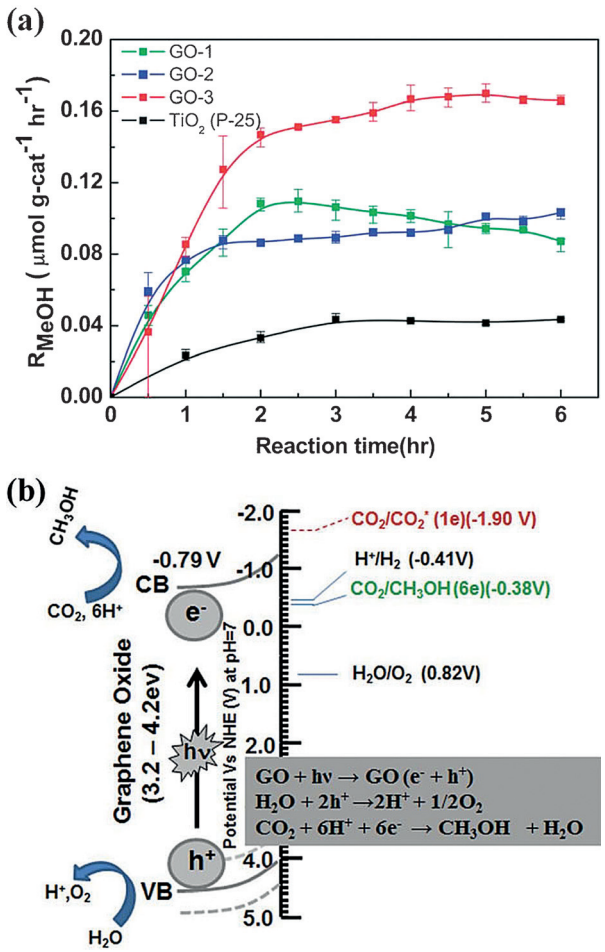

Figure 7. a) Photocatalytic methanol formation on different graphene oxide samples (GO-1, GO-2, GO-3) and P25 under simulated solar-light irradiation; b) Schematic illustration of photocatalytic reduction mechanism of CO_2 on graphene oxide. Reprinted with permission from Ref. [68]. Copyright 2013, Royal Society of Chemistry.

3. Photocatalyitc Hydrogen Generation

Hydrogen (H_2), as a storable and clean fuel, is regarded as an ideal energy-source carrier for the future owing to its high energy capacity and environmental friendliness.[69–73] Since Fujishima and Honda first discovered the evolution of O_2 and H_2 through the photoelectrochemical splitting of water on the surface of TiO_2 and Pt electrodes, respectively,[2] H_2 production from solar water splitting using semiconductor photocatalysts has attracted extensive attention.[74–81] Although great progress has been made in the photocatalytic hydrogen generation, current conversion efficiencies on semiconductor photocatalysts for solar hydrogen production are still low for the practical application and commercial benefit. Further research efforts towards highly active semiconductor photocatalysts for photocatalytic hydrogen generation are ongoing.

Considering the superior electrical properties and unique 2D conjugated structure of graphene, it is of great interest to combine semiconductor photocatalysts with graphene. In fact, the role of graphene in enhancing photocatalytic H_2 production has been extensively investigated for photocatalysts.[82–85] In the following Sections, the beneficial aspects of graphene-based photocatalysts in boosting the efficiency of solar energy conversion will be illustrated, including graphene as electron acceptor and transporter, co-catalyst, photosensitizer, coupler, and photocatalyst.

3.1. Graphene as an Electron Acceptor

One of the fundamental issues in photocatalysis is the fast recombination of photogenerated electron–hole pairs within the photocatalysts. Therefore, suppressing the recombination of electron–hole pairs is one of the key factors to improve the photocatalytic activities of photocatalysts. In recent years, a variety of semiconductor photocatalysts have been combined with graphene to suppress the recombination of electron–hole pairs to enhance photocatalytic H_2 production.[41,82,86–95] For example, Zhang et al.[86] reported a series of composites consisting of TiO_2 and graphene prepared by a sol–gel method as an efficient photocatalyst for H_2 production. The TiO_2/graphene composite photocatalysts showed enhanced photocatalytic H_2 production in Na_2S-Na_2SO_3 aqueous solutions under Xe lamp irradiation. The photocatalytic activity of the optimal TiO_2/graphene composite exceeds that of P25 TiO_2 by more than 1.9 times. The enhanced photocatalytic activity is ascribed to the presence of graphene, which acts as an electron acceptor and transporter to efficiently separate the photogenerated electron–hole pairs in the TiO_2 nanoparticles. However, it should be noted that the role of graphene as an electron acceptor is significantly affected by the interfacial interaction between graphene and TiO_2. It has been reported that a simple mechanical mixture of graphene and TiO_2 cannot enhance the photocatalytic activity of TiO_2 owing to the poor interfacial interaction between graphene and TiO_2, which makes it difficult to transfer the photoexcited electrons from TiO_2 into graphene.[19,40] Therefore, a strong interfacial interaction between graphene and TiO_2 is crucial for the improvement of interfacial charge transfer and enhancement of photocatalytic activity.

Besides TiO_2, the coupling of graphene and some other semiconductor photocatalysts has also been explored. Li et al.[84] fabricated visible-light-driven graphene/CdS nanocomposite photocatalysts, achieving a high efficiency of the photocatalytic H_2 production from lactic acid in aqueous solution. In another research, reduced graphene oxide was incorporated into $BiVO_4$ to form $BiVO_4$/RGO composite films.[42] The excellent electronic conductivity of graphene in the $BiVO_4$/RGO composite film promoted the electron transport from $BiVO_4$ to the electrode, leading to a minimized charge recombination and the enhanced activity for the photoelectrochemical water splitting. Surprisingly, a 10-fold enhancement was observed on $BiVO_4$/RGO composite film compared with pure $BiVO_4$ film at a 0.8 V bias under visible-light illumination. To further explore the potential application of graphene based-photocatalysts in hydrogen production, Mukherji et al.[96] reported that graphene sheets coupled on $Sr_2Ta_2O_{7-x}N$ can acted as a conductive electron transport "highway" to facilitate the charge-carrier migration for increased photocatalytic H_2 production. Similarly, by using graphene as an electron acceptor/transporter, graphene/g-C_3N_4 composites showed a high H_2 evolution rate under visible light irradiation.[72] The H_2-production rate of the graphene/g-C_3N_4 composite with the optimal graphene content exceeds that of pure g-C_3N_4 by more than three times under the same reaction conditions. Interestingly, the dye molecules were also used as a photocatalyst or photosensitizer to construct a graphene/dye photocatalytic H_2-evolution system.[97,98] As shown in Figure 8, in this system, dye

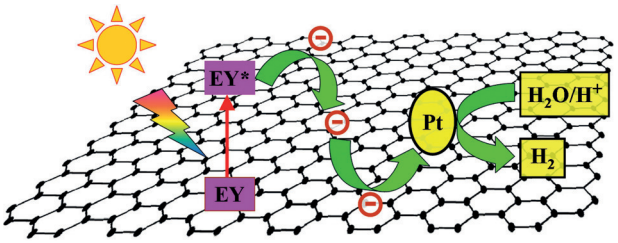

Figure 8. Schematic illustration of the proposed mechanism for photocatalytic H_2 production on the dye molecules eosin Y –graphene/Pt photocatalyst under visible-light irradiation.

molecules as the photocatalyst were excited to generate electron–hole pairs under visible-light irradiation. The photogenerated electrons on the excited dye molecules can transfer to the surface of the co-catalyst (Pt) through graphene sheets and then promote photocatalytic H_2 evolution.

To further investigate the role of graphene as an electron acceptor in photocatalytic H_2 evolution, Kim et al.[99] developed a new type of self-assembled core–shell reduced nanosized graphene oxide (r-NGOs)/TiO_2 structure. The surface of the TiO_2 nanoparticles in the r-NGOs/TiO_2 composites were well wrapped and fully contacted by r-NGOs to form the unique core–shell nanoarchitecture. As shown in Figure 9, the

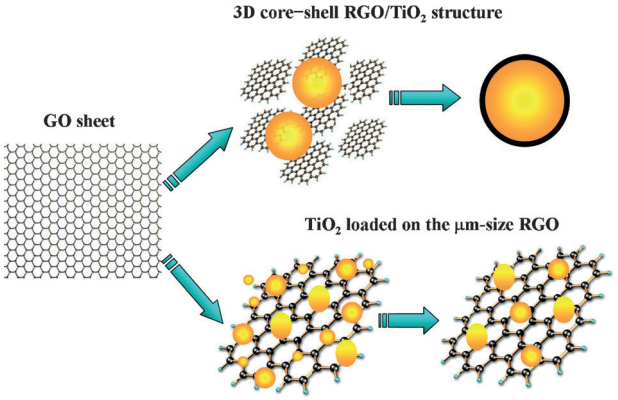

Figure 9. Schematic illustration of the contact interface of the 3D core–shell RGO/TiO_2 structure and TiO_2 loaded on micrometer-size RGO.

core–shell structure composite provides a three-dimensional intimate contact and a strong interaction between r-NGOs and TiO_2, resulting in a highly efficient electron transfer on the surface of r-NGOs. As a result, an enhancement of the photocatalytic activity in the hydrogen and photocurrent generation was observed on the r-NGOs/TiO_2 composites. This work implies that the contact area and the interfacial interaction between graphene and photocatalysts play an important role for graphene as an electron acceptor in graphene-enhanced photocatalytic H_2 evolution.

Interestingly, the role of graphene as an electron acceptor affects not only the transfer of electrons in graphene/semiconductor composites, but also shifts the conduction-band potential of the semiconductor in the composite. Usually, for effective photocatalytic H_2 evolution, the conduction-band potential of the semiconductor should be more negative than the reduction potential (H^+/H_2). Bi_2WO_6 as an important photocatalyst has a relatively narrow band gap and is not a suitable candidate for photocatalytic H_2 evolution because it has a less-negative conduction-band potential than H^+/H_2.[56,100] Surprisingly, Sun et al.[100] reported a graphene/Bi_2WO_6 nanocomposite as a highly efficient visible-light-driven photocatalysts for both H_2 and O_2 generation. In this system, the graphene in the graphene/Bi_2WO_6 nanocomposite served as an electron acceptor to promote the separation of photogenerated electron–hole pairs in Bi_2WO_6. In addition, in the nanocomposite, which comprises a homogeneous dispersion of Bi_2WO_6 nanoparticles on the graphene surface, the formation of W-O-C bonds elevates the Fermi level of the graphene/Bi_2WO_6 composite and decreases its conduction-band potential. The strong chemical covalent bonding facilitates the electronic interaction and charge equilibration between graphene and Bi_2WO_6, resulting in a more negative reduction potential than H^+/H_2. Therefore, a high rate of H_2 production was obtained on the graphene/Bi_2WO_6 composite photocatalyst.

Besides the role of graphene as an electron acceptor in semiconductor heterojunction systems, graphene can be used as a solid-state electron mediator for water splitting in an ingenious Z-scheme photocatalysis system. Since the first report on a Z-scheme photocatalyst stoichiometrically splitting of water into H_2 and O_2 was published in 1997 by Sayama et al.,[101] Z-Scheme photocatalysis systems have demonstrated a large potential application in efficient solar-energy conversion.[102–106] Usually, an electron-shuttle mediator between two different photocatalysts in the Z-scheme system plays a critical role in enhancing the efficiency of photocatalytic splitting of water. Many efforts have been made to develop an electron mediator (such as, Fe^{3+}/Fe^{2+} and IO_3^-/I^- couples) for effective Z-scheme photocatalytic water splitting system.[103] Recently, it was found that graphene could act as a solid-state electron mediator for water splitting in the Z-scheme photocatalysis owing to its unique electronic features. For example, Iwase et al.[104] demonstrated that RGO functioned as a solid-state electron mediator improving the photocatalytic activity for a Z-scheme water-splitting system consisting of Ru/$SrTiO_3$:Rh and $BiVO_4$ as the H_2 and O_2 evolution photocatalysts, respectively. As shown in Figure 10, RGO in this Z-scheme system can transfer the photogenerated electrons from the conduction band of $BiVO_4$ to Ru/$SrTiO_3$:Rh under visible-light illumination. Thus Ru as the co-catalyst can catalyze the reduction of water to H_2 by the electrons in Ru/$SrTiO_3$:Rh, while the holes leaving in the valence band of $BiVO_4$ can oxidize water to O_2, accomplishing a complete cycle of Z-scheme photocatalytic water splitting. Notably, they found that the reduction extent and the hydrophobicity of GO as an electron mediator had a great influence on the electron transfer in the Z-scheme system. With the right balance of GO reduction and a high level of GO hydrophilicity, the (Ru/$SrTiO_3$:Rh)-(RGO/$BiVO_4$) system showed a much higher photocatalytic H_2-production rate, than the rate obtained over the system without RGO ((Ru/$SrTiO_3$:Rh)-$BiVO_4$). Therefore, the balance between the extent of GO reduction and the hydrophobicity exhibits clear influence on the photocatalytic activity in this kind of system. In addition, it should be noted that the contact interface and strong interaction between photocatalyst-mediator-photocatalyst are crucial for developing an effective Z-scheme photocatalytic water-splitting system. Nevertheless, this work shows graphene can function as an effective solid-state electron mediator for water splitting in Z-scheme photocatalysis systems, which provides a new way for the design and development of efficient photocatalytic systems for overall water splitting.

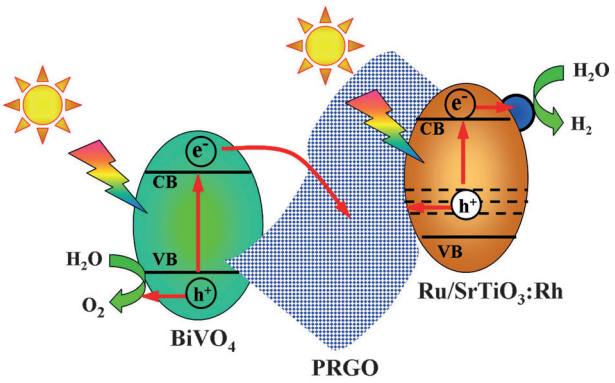

Figure 10. Schematic illustration of the proposed mechanism of photocatalytic water splitting in the Z-scheme (Ru/$SrTiO_3$:Rh)-(PRGO/$BiVO_4$) system under visible light irradiation. PRGO = photoreduced graphene oxide

3.2. Graphene as a Co-Catalyst

Usually, the loading of noble metal (such as Pt, Au, and Pd) onto the semiconductor surface is an efficient strategy to improve the photocatalytic hydrogen production efficiency. This is because these noble metals have a higher work function than most semiconductors, promoting the transfer of photogenerated electrons from the semiconductor to noble metal, thereby decreasing the recombination of electrons and holes. However, these noble metals are both expensive and rare. Therefore, many efforts have been made to develop low-cost co-catalysts,[107–109] for example, N-graphene as a co-catalyst in the N-graphene/CdS composites also can prevent CdS from photocorroding in Na_2S/Na_2SO_3 solution under

visible-light irradiation.[109] Considering the work function of graphene and the different reduction potentials of diverse semiconductor photocatalysts, it is still difficult to develop graphene treatments for all the possible photocatalysts for photocatalytic hydrogen production. Recently, Zhang et al.[61] reported a high efficiency of the solar photocatalytic H_2 production over a reduced graphene oxide (RGO)/$Zn_xCd_{1-x}S$ nanocomposite. Surprisingly, the optimized RGO/$Zn_{0.8}Cd_{0.2}S$ photocatalyst had the apparent quantum efficiency (QE) of 23.4% at 420 nm even in the absence of noble-metal co-catalysts, which is better than that of Pt-loaded $Zn_{0.8}Cd_{0.2}S$ photocatalysts, with an optimized Pt content, under the same experimental conditions. As shown in Figure 11, the RGO co-

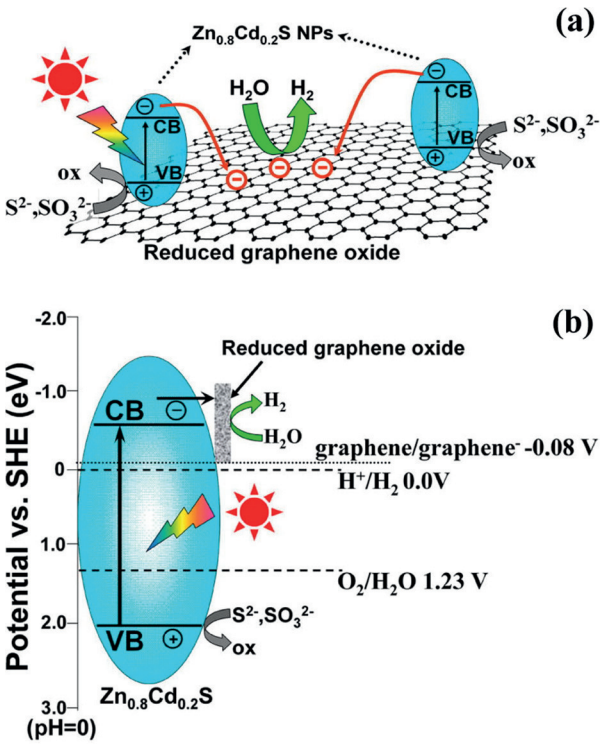

Figure 11. a) Schematic illustration of the charge transfer and separation in the RGO/$Zn_{0.8}Cd_{0.2}S$ system under simulated solar irradiation. b) Schematic illustration of the proposed mechanism for photocatalytic hydrogen production on the RGO/$Zn0_{.8}Cd_{0.2}S$ system under simulated solar irradiation. Reprinted with permission from Ref. [61]. Copyright 2012, American Chemical Society.

catalyst played a dual role in enhancing photocatalytic H_2-production activity: the RGO sheets accumulated the photogenerated electrons on its surface, leading to the separation of hole–electron pairs. In addition the carbon atoms on the surface of the RGO sheets can catalyze the reduction of H^+ to H_2 molecule, through the accumulation of the photogenerated electrons they have a more negative reduction potential than H^+/H_2. Subsequent photoelectrochemical measurements further confirmed the beneficial role of RGO in enhanced photocatalytic activity.

3.3. Graphene as a Photosensitizer

Graphene is widely used as a support for photocatalysts to accept and transport the photogenerated electrons from the photocatalysts.[38,110–120] Recently, much effort has been made for developing visible-light-responsive photocatalysts by using graphene as a photosensitizer.[121–130] For example, Zeng et al.[122] reported that GO/TiO_2 nanocomposites prepared by a hydrothermal method showed high visible-light photocatalytic H_2-production activity in which GO functioned as a photosensitizer. The subsequent mechanism for visible-light-driven H_2 evolution was proposed that GO was photoexcited to produce the electron–hole pairs. These excited electrons were subsequently injected into the conduction band of TiO_2 and then were transferred to the active sites on the GO/TiO_2 nanocomposite for reducing water molecules or proton to produce H_2. Very recently, Li et al.[128] constructed ternary CdS/reduced graphene oxide/TiO_2 nanotube arrays hybrids. They found that the reduced graphene oxide in the middle layer not only acted as an electron acceptor, but also served as a photosensitizer for further increasing photon capture. The above results clearly demonstrate that graphene can serve as photosensitizer to expand the spectral responsive range of wide-band-gap semiconductors to visible light. In fact, some theoretical calculations also show that graphene can potentially act as a photosensitizer in some wide-band-gap semiconductor/graphene composites.[26,130] For example, Du et al.[26] used large-scale density functional theory (DFT) calculations to study the interfacial charge transfer between graphene and rutile TiO_2. They found that electrons could be directly excited from the upper valence band of graphene to the conduction band of TiO_2 under visible light irradiation, which was in accordance with the experimental wavelength-dependent photocurrent generation of the graphene/TiO_2 photoanode. These results demonstrated the photoinduced electrons in graphene could be successfully injected into the conduction band of semiconductors, thus producing the visible-light activity.

3.4. Coupling Multiple Photocatalysts with Graphene to Construct Ternary Composites

Graphene-based binary photocatalyst composites have many advantages over the same single photocatalyst in photocatalytic hydrogen evolution. Recently, graphene-based ternary composite photocatalysts have attracted a lot of attention in photocatalytic hydrogen evolution.[19,131–139] Compared to the binary composite system, the graphene-based ternary composites using genuine heterostructure constituents show an enhanced photocatalytic H_2 production because a favorable band alignment gives efficient separation of charge carriers. Some graphene-based ternary systems, such as TiO_2/MoS_2/graphene,[19] TiO_2/Pt/graphene,[131] Cu/TiO_2/graphene,[132] ZnS/MoS_2/graphene,[133] CdS/TaON/RGO,[134] ZnO/CdS/RGO,[135] CdS/MoS_2/graphene,[136,137] g-C_3N_4/MoS_2/graphene,[138] and NiS/$Zn_xCd_{1-x}S$/RGO,[139] have been reported to give a significant enhancement of photocatalytic H_2 production. For example, Jia et al.[137] reported

CdS and MoS_2 nanocrystals dispersed on graphene sheets as an efficient photocatalyst for solar hydrogen production from water splitting. It was shown that the photocatalytic H_2-production efficiency of CdS was dramatically enhanced by using graphene and MoS_2 as co-catalysts. Compared to the solar photocatalytic activity of the binary CdS/MoS_2 and CdS/graphene composite photocatalysts, the H_2 production rate of ternary CdS/MoS_2/graphene composites was 2 and 14.7 times greater, respectively. The reason for the enhanced photocatalytic activity is that the photogenerated electrons from CdS can transfer to MoS_2 through the two-dimensional carbon network of graphene, leading to the effective separation of electron–hole pairs in CdS. The photogenerated electrons accumulating on the edge sites of MoS_2 can catalyze the reduction of H^+ to H_2 on the surface of MoS_2. Subsequently, Jia et al. utilized time-resolved photoluminescence techniques to investigate the charge-transfer properties at the CdS/MoS_2/graphene composite interface and to confirm the proposed mechanism. Indeed, coupling multiple photocatalysts with graphene to construct ternary composites can improve the photocatalytic performance.[131–139] However, it should be noted that the proper choice of the constituent photocatalyst in graphene-based ternary composites and the strong interfacial interaction between their constituent materials are crucial for enhancing the photocatalytic properties. The enhancement results from the formation of the beneficial band alignment and the efficient separation of charge carriers at different levels.

Recently, Zhang et al.[139] reported ternary NiS/$Zn_xCd_{1-x}S$/RGO nanocomposites with enhanced solar photocatalytic H_2-production activity. Interestingly, in this ternary system, the co-loading of both a water-reduction co-catalyst and a water-oxidation co-catalyst on the $Zn_xCd_{1-x}S$ can significantly improve the photocatalytic water-splitting activity. As shown in Figure 12, RGO in the ternary composite acted as an electron acceptor and transporter to separate the photogenerated electron–hole pairs in $Zn_xCd_{1-x}S$, and an efficient water-reduction co-catalyst to provide the reduction active site for H_2 generation. NiS as an oxidation active site in the ternary composite can accumulate the photogenerated holes in $Zn_xCd_{1-x}S$ because of the effect of nanoscale p–n junctions between NiS and $Zn_xCd_{1-x}S$, and then facilitate the consumption of the photogenerated holes by sacrificial reagents. The subsequent electrochemical impedance spectra and transient photocurrent response results further confirmed that the proposed mechanism was correct. Therefore, the a higher solar photocatalytic H_2-production rate was observed over ternary NiS/$Zn_xCd_{1-x}S$/RGO nanocomposites than over the binary NiS/$Zn_xCd_{1-x}S$ and $Zn_xCd_{1-x}S$/RGO nanocomposites under the same measured conditions. It is noteworthy that the H_2-production rate of the ternary NiS/$Zn_{0.5}Cd_{0.5}S$/RGO nanocomposite photocatalyst reached 375.7 μmol h^{-1} with 31.1 % apparent quantum efficiency at 420 nm, representing one of the most highly active metal sulfide photocatalysts in the absence of noble metal co-catalysts. This high H_2-production rate even exceeded the rate obtained over the optimized Pt/$Zn_{0.5}Cd_{0.5}S$ sample under the same reaction conditions. This work shows that the co-loading of both water-reduction and water-oxidation co-catalysts on the semiconductor is an efficient strategy to improve the photocatalytic H_2-production activity, which provides new physicochemical insight for the design and development of graphene-based multicomponent photocatalysts for solar-conversion applications.

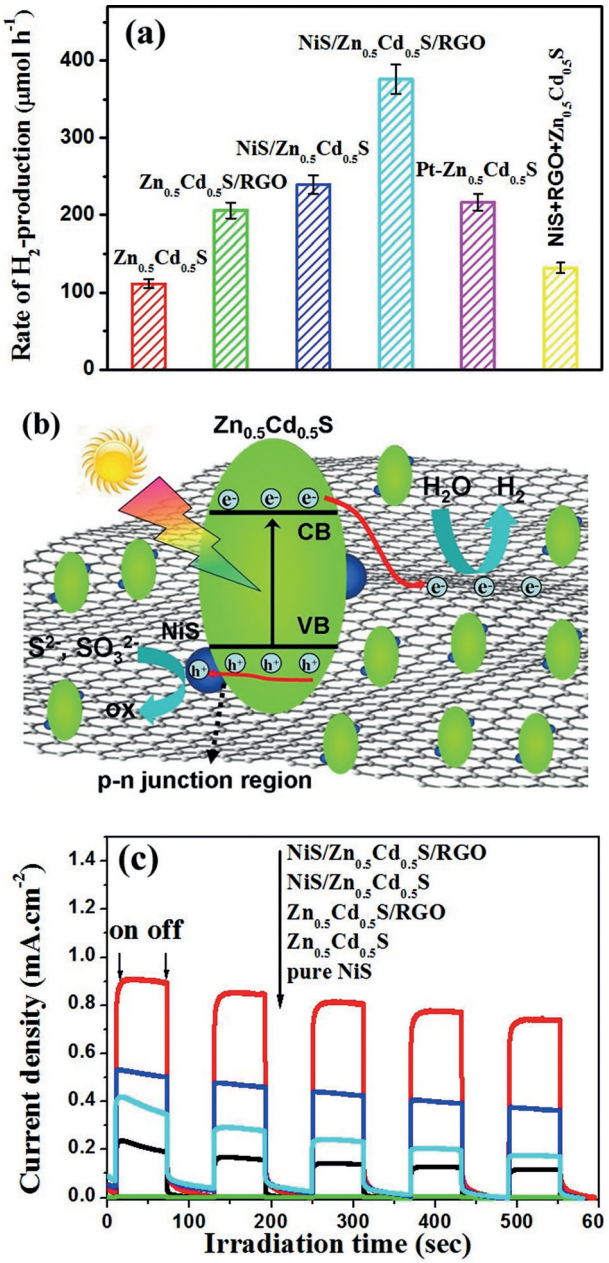

Figure 12. a) Comparison of photocatalytic H_2-production activity of the $Zn_{0.5}Cd_{0.5}S$, NiS/$Zn_{0.5}Cd_{0.5}S$, $Zn_{0.5}Cd_{0.5}S$/RGO, and NiS/$Zn_{0.5}Cd_{0.5}S$/RGO samples under simulated solar irradiation; b) Schematic illustration of the proposed mechanism for the enhanced photocatalytic H_2 production on the NiS/$Zn_{0.5}Cd_{0.5}S$/RGO composite under simulated solar irradiation; c) Transient photocurrent responses of the pure NiS, $Zn_{0.5}Cd_{0.5}S$, $Zn_{0.5}Cd_{0.5}S$/RGO, NiS/$Zn_{0.5}Cd_{0.5}S$, and NiS/$Zn_{0.5}Cd_{0.5}S$/RGO samples under simulated solar irradiation. Reprinted with permission from Ref. [139]. Copyright 2014, Wiley-VCH.

In addition to the strategy of co-loading reduction and oxidation co-catalysts on graphene-based ternary composites,

another approach is to extend the light response from UV to visible light and to near-infrared light by using suitable constituent materials in graphene-based ternary composites. Generally, visible light and near-infrared light take over 45% and 50% of the solar light energy, respectively. In view of the efficient utilization of solar energy, it is highly desirable to develop visible-light and near-infrared-light responsive photocatalytic systems. One way to achieve this could be with graphene-based multicomponent composites with a suitable near-infrared-light responsive photocatalyst and a visible-light-active semiconductor. But much effort is required for the development of graphene-based multicomponent composites for full solar-light photocatalytic H_2 production.

3.5. Graphene as p- or n-Type Semiconductor in p–n Heterojunctions

The use of p–n heterojunctions in solar cell has been widely considered to separate light-induced electrons and holes. In p–n heterojunctions with a space charge region, the inner electric fields can drive the electrons and holes to move in opposite directions, giving an effective separation of electron–hole pairs. Thus using semiconductor composites with p–n heterojunction may lead to enhanced photocatalytic efficiency.[140,141] Moreover, it was found that graphene oxide could serve as either a p-type or n-type semiconductor because its structure and electronic properties can be tuned by changing the composition of its oxygen functional groups.[142–145] For instance, replacing oxygen functional groups on the graphene oxide sheet with electron-donating nitrogen functionalities can transform graphene oxide into an n-type semiconductor. Meanwhile, graphene oxide can also become a p-doped material because oxygen atoms have a higher electronegativity than carbon atoms. More importantly, graphene oxides with p- or n-type semiconductor characteristics are potential semiconductor photocatalysts for photocatalytic H_2 production or water oxidation, respectively. Recently, a visible-light-response GO/TiO_2 composite photocatalyst with a p–n heterojunction was reported, and the GO was shown to act as either a p-type or n-type semiconductor in the composite.[142] By changing the GO concentrations in the starting synthesis solutions, GO in the composite shows p- or n-type semiconductor characteristics for wavelength-dependent photocurrent conversion. Especially, when p-type semiconductor behavior was observed for the GO in the GO/TiO_2 composite, the formation of the p–n heterojunction in the composite can facilitate the separation of photogenerated carriers, resulting in enhanced photocatalytic activity.

Very recently, Wu and co-workers[144] reported a nanoscale p–n junction photocatalyst consisting of p-type MoS_2 and n-type RGO. In this study, the p-MoS_2/n-RGO junction played the main role in significantly improving the photocatalytic H_2-production activity. The proposed mechanism for the effect of the p–n junction is illustrated in Figure 13. Under visible-light irradiation, p-MoS_2 and n-RGO were excited to generate electron–hole pairs. The photogenerated electrons from the nanoplatelet p-MoS_2 with higher-energy states could be transported to the n-RGO, while the photogenerated holes

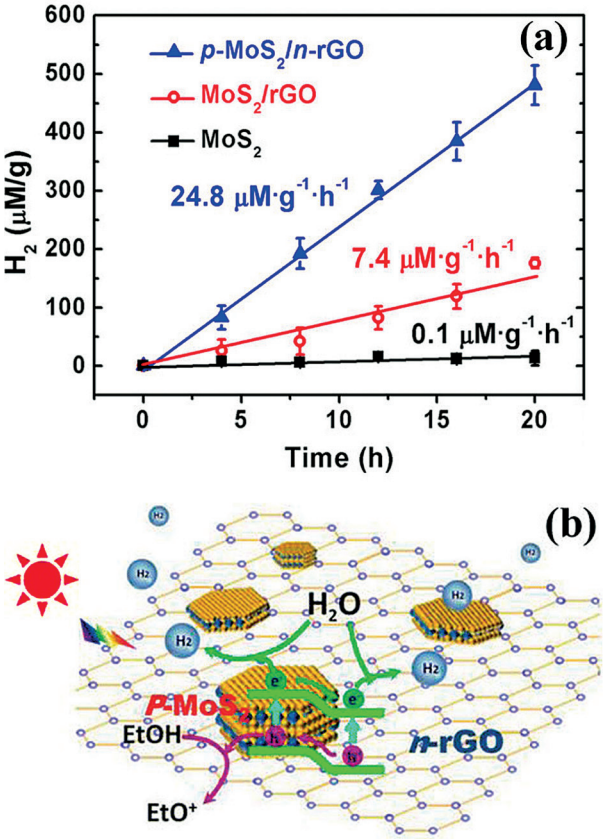

Figure 13. a) Comparison of the photocatalytic H_2-production activity on the three types of particulate photocatalysts, including the solitary MoS_2, the MoS_2/rGO composite, and the p-MoS_2/n-rGO junction; b) Schematic illustration of the charge transfer and separation in the p-MoS_2/n-rGO photocatalysts under simulated solar-light irradiation. Reprinted with permission from Ref. [144]. Copyright 2013, American Chemical Society.

in the n-RGO were transported by the inner electric field of the p–n junction to p-MoS_2 which has a higher valance band. In this case, the photogenerated electron–hole pairs are effectively separated by the p–n junction between MoS_2 and RGO, resulting in the enhanced photocatalytic H_2-production efficiency. These results clearly demonstrate another potential role of RGO as a p- or n-type semiconductor in p–n heterojunctions for solar-energy conversion.

3.6. Graphene as a Photocatalyst

In addition to its role in graphene-based composites for photocatalytic H_2 production, graphene oxide itself can also serve as a photocatalyst for hydrogen production from water splitting.[27,143,146] It has also been reported that graphene oxide can act as a p- or n-type semiconductor depending on the degree of oxidation.[143] Therefore, the potential of graphene oxide as a photocatalyst may be developed by varying the oxidation level. Considering the uncontrollable surface structure of graphene oxide at the present stage, it is not easy to develop graphene oxide as a photocatalyst for hydrogen production. Recently, Yeh et al.[27] reported a GO

specimen semiconductor with a band gap of 2.4–4.3 eV as a photocatalyst for hydrogen production from an aqueous methanol solution under mercury lamp illumination. It was found that a steady evolution of H_2 was observed over the GO specimen even in the absence of Pt co-catalyst. This is because with a sufficient degree of oxidation the GO has a conduction band edge level higher than the redox potential of H^+/H_2. Under illumination, the photogenerated electrons from the carbon atoms can be approached by protons, which are then reduced into hydrogen molecules. Very recently, the same group[143] reported nitrogen-doped GO quantum dots (NGO-QDs) as an efficient photocatalyst for stoichiometrically splitting water into H_2 and O_2 under solar light illumination. The NGO-QDs photocatalyst with a band gap of 2.2 eV consists of stacked nitrogen-doped graphene sheets with external oxygen functional groups. The structure gives rise to p–n type photochemical diodes which respond to visible light. This novel NGO-QDs construction with p-type and n-type conductivity can catalyze H_2 and O_2 evolution from water splitting under visible-light irradiation. Moreover, the NGO-QDs photocatalyst is chemically stable during the photocatalytic process, suggesting it acts in a sustainable and environmentally friendly way. Since the electronic properties of graphene oxide depend on the degree of oxidation, tuning its oxidation level is expected to enhance its activity in the photocatalytic production of H_2. However, the control of the oxidation level of graphene oxide is a complicated process. Further efforts have to be developed for preparing high-quality graphene oxide sheets with tunable oxidation level. Nevertheless, the above findings demonstrate that graphene species, as metal-free, cost-effective, and environmentally friendly materials, are promising photocatalysts for overall water-splitting under solar illumination.

4. Conclusion and Outlook

In recent years much progress has been made in constructing graphene-based photocatalysts for solar-fuel generation. In this Review, we have summarized the recent advances in developing efficient graphene-based photocatalysts for the photocatalytic reduction of CO_2 to hydrocarbon fuels and the photocatalytic hydrogen production from water splitting. Many studies have demonstrated that the introduction of graphene into various semiconductor photocatalysts can improve the efficiency of CO_2 conversion and the rate of H_2 production. This improvement is due to the unique 2D structure and the excellent electronic properties of graphene that result in the enhanced separation/migration of photogenerated electrons and holes, extended the light absorption range, allow noble metals to be replaced as co-catalysts and allow graphene to catalyze the hydrogen evolution by itself. Although considerable progress has been achieved, there are still many challenges in the exploitation of highly activity graphene-based photocatalysts for solar-fuel generation.

First, large-scale production of graphene-based photocatalysts with high and uniform quality is still challenging. As we know, the photocatalytic performance of photocatalysts is highly dependent on their composition and morphology. To achieve high performance, graphene-based photocatalysts with controlled morphologies and compositions are required. For example, the well-defined 2D structure of graphene allows face-to-face orientation and an intimate contact between layered photocatalysts and graphene sheets, which facilitates the separation of photogenerated charge carriers, thus enhancing photocatalytic activity in photocatalytic solar-fuel generation.[147] The 3D nanostructure of graphene-based photocatalysts can maximize the interaction between the two composites, which will extremely enhance the conversion efficiency of solar energy. In addition, multicomponent graphene-based photocatalysts have a remarkable ability to facilitate the charge separation at different levels by the proper choice of band-gap width in the constituent materials. Therefore, more efficient synthetic strategies need be developed for preparing graphene-based photocatalysts with controlled morphologies and compositions for the enhanced performance.

Secondly, the efficiencies of solar-fuel production based on graphene-based photocatalysts are still low in most photocatalytic systems. For the photocatalytic CO_2 conversion, at present only a 1% solar energy to fuel efficiency is achieved for coupled water oxidation and CO_2 reduction.[8] One of the key factors limiting the efficiency is a lack of suitable photocatalysts with ideal band-gap characteristics. In contrast to CO_2 conversion, the photocatalytic H_2-production efficiency of graphene-based photocatalysts is relatively high. However, the H_2-production efficiency from the overall water-splitting in pure water is still significantly below the theoretical maxima. Most graphene-based photocatalysts for H_2 evolution are based on the water-splitting half-reactions with sacrificial reagents. Only a few graphene-based photocatalysts for H_2 evolution by overall water-splitting have been reported. For example, Amal et al.[104] developed a (Ru/$SrTiO_3$:Rh)-(RGO/$BiVO_4$) Z-scheme water splitting system, which can reduce water to H_2 and oxidize water to O_2 for overall water-splitting under visible light irradiation. In this regard, the development of graphene-based Z-scheme photocatalysis systems is desirable to improve the photocatalytic H_2-production efficiency of overall water-splitting in pure water.

Thirdly, the underlying mechanism of photocatalytic activity enhancement in solar-fuel generation by graphene-based photocatalysts is still not well understood. Especially, the photocatalytic reduction of CO_2 to fuels involves multi-electron transfer processes and various redox potentials. Thus, a variety of products can be formed in the photocatalytic CO_2 conversion by the preferential redox potentials of the photogenerated carriers, and the products selectivity is associated with the chemical pathways of CO_2 reduction. Therefore, the functions of graphene in the photocatalytic CO_2 conversion need to be better studied to improve the selectivity for the specific fuel. Furthermore, a detailed comparison of the roles of graphene in the photocatalytic CO_2 conversion and in the widely studied photocatalytic hydrogen production from water splitting should be carried out. Recently, graphene has been extensively applied to improve the photocatalytic H_2-production performance and its roles in photocatalytic hydrogen generation have been well summarized. However,

the studies on the graphene-based photocatalysts for reduction of CO_2 are at an early stage and some essential functions of graphene in the enhancement of photocatalytic CO_2 conversion are not well clarified. Therefore, the comparison of the functions of graphene in the photocatalytic CO_2 conversion and H_2 generation is necessary for a better understanding on the unique contribution of graphene in these processes. In addition, the underlying mechanism of action of graphene and its related species as a photocatalyst for CO_2 reduction to methanol and H_2 evolution from water splitting should be further clarified. Electrochemical analysis has already demonstrated that graphene and its related species can exhibit both p- and n-type conductivities by modulating its oxidation degree. Theoretical calculations may be able to simulate the electronic structural characteristics of graphene and its related species, and provide us with in-depth insight into their semiconductor properties. Nevertheless, the deepening of our understanding of the underlying mechanistic aspects should lead to substantial breakthroughs for solar-fuel generation by graphene-based photocatalysts.

This work was supported by the 973 program (2013CB632402), NSFC (21403079, 51272199, 51320105001, 21433007, and 21177100), and Deanship of Scientific Research (DSR) of King Abdulaziz University (90-130-35-HiCi).

How to cite: *Angew. Chem. Int. Ed.* **2015**, *54*, 11350–11366
Angew. Chem. **2015**, *127*, 11508–11524

[1] P. D. Tran, L. H. Wong, J. Barber, J. S. C. Loo, *Energy Environ. Sci.* **2012**, *5*, 5902.
[2] A. Fujishima, K. Honda, *Nature* **1972**, *238*, 37.
[3] T. Inoue, A. Fujishima, S. Konishi, K. Honda, *Nature* **1979**, *277*, 637.
[4] A. Kudo, Y. Miseki, *Chem. Soc. Rev.* **2009**, *38*, 253.
[5] X. B. Chen, S. H. Shen, L. J. Guo, S. S. Mao, *Chem. Rev.* **2010**, *110*, 6503.
[6] W. Q. Fan, Q. H. Zhang, Y. Wang, *Phys. Chem. Chem. Phys.* **2013**, *15*, 2632.
[7] P. V. Kamat, J. Bisquert, *J. Phys. Chem. C* **2013**, *117*, 14873.
[8] A. J. Cowan, J. R. Durrant, *Chem. Soc. Rev.* **2013**, *42*, 2281.
[9] K. F. Li, X. Q. An, K. H. Park, M. Khraisheh, J. W. Tang, *Catal. Today* **2014**, *224*, 3.
[10] M. R. Hoffmann, J. A. Moss, M. M. Baum, *Dalton Trans.* **2011**, *40*, 5151.
[11] A. J. Morris, G. J. Meyer, E. Fujita, *Acc. Chem. Res.* **2009**, *42*, 1983.
[12] H. Q. Sun, S. B. Wang, *Energy Fuels* **2014**, *28*, 22.
[13] X. Nie, M. R. Esopi, M. J. Janik, A. Asthagiri, *Angew. Chem. Int. Ed.* **2013**, *52*, 2459; *Angew. Chem.* **2013**, *125*, 2519.
[14] A. D. Handoko, J. W. Tang, *Int. J. Hydrogen Energy* **2013**, *38*, 13017.
[15] S. Rawalekar, T. Mokari, *Adv. Energy Mater.* **2013**, *3*, 12.
[16] I. V. Lightcap, T. H. Kosel, P. V. Kamat, *Nano Lett.* **2010**, *10*, 577.
[17] G. Williams, B. Seger, P. V. Kamat, *ACS Nano* **2008**, *2*, 1487.
[18] H. Zhang, X. J. Lv, Y. M. Li, Y. Wang, J. H. Li, *ACS Nano* **2010**, *4*, 380.
[19] Q. J. Xiang, J. G. Yu, M. Jaroniec, *J. Am. Chem. Soc.* **2012**, *134*, 6575.
[20] Q. J. Xiang, J. G. Yu, M. Jaroniec, *Chem. Soc. Rev.* **2012**, *41*, 782.
[21] G. C. Xie, K. Zhang, B. D. Guo, Q. Liu, L. Fang, J. R. Gong, *Adv. Mater.* **2013**, *25*, 3820.
[22] I. V. Lightcap, P. V. Kamat, *Acc. Chem. Res.* **2013**, *46*, 2235.
[23] K. S. Novoselov, A. K. Geim, S. V. Morozov, D. Jiang, Y. Zhang, S. V. Dubonos, I. V. Grigorieva, A. A. Firsov, *Science* **2004**, *306*, 666.
[24] T. N. Lambert, C. A. Chavez, N. S. Bell, C. M. Washburn, D. R. Wheeler, M. T. Brumbach, *Nanoscale* **2011**, *3*, 188.
[25] Y. H. Ng, A. Iwase, N. J. Bell, A. Kudo, R. Amal, *Catal. Today* **2011**, *164*, 353.
[26] A. J. Du, Y. H. Ng, N. J. Bell, Z. H. Zhu, R. Amal, S. C. Smith, *J. Phys. Chem. Lett.* **2011**, *2*, 894.
[27] T. F. Yeh, J. M. Syu, C. Cheng, T. H. Chang, H. S. Teng, *Adv. Funct. Mater.* **2010**, *20*, 2255.
[28] X. Q. An, J. C. Yu, *RSC Adv.* **2011**, *1*, 1426.
[29] L. Han, P. Wang, S. J. Dong, *Nanoscale* **2012**, *4*, 5814.
[30] N. Zhang, Y. H. Zhang, Y. J. Xu, *Nanoscale* **2012**, *4*, 5792.
[31] Q. J. Xiang, J. G. Yu, *J. Phys. Chem. Lett.* **2013**, *4*, 753.
[32] Y. H. Ng, S. Ikeda, M. Matsumura, R. Amal, *Energy Environ. Sci.* **2012**, *5*, 9307.
[33] H. X. Chang, H. K. Wu, *Energy Environ. Sci.* **2013**, *6*, 3483.
[34] D. Chen, H. Zhang, Y. Liu, J. H. Li, *Energy Environ. Sci.* **2013**, *6*, 1362.
[35] N. J. Bell, H. N. Yun, A. J. Du, H. Coster, S. C. Smith, R. Amal, *J. Phys. Chem. C* **2011**, *115*, 6004.
[36] Q. J. Xiang, D. Lang, T. T. Shen, F. Liu, *Appl. Catal. B* **2015**, *162*, 196.
[37] Y. H. Zhang, Z. R. Tang, X. Z. Fu, Y. J. Xu, *ACS Nano* **2010**, *4*, 7303.
[38] S. D. Perera, R. G. Mariano, K. Vu, N. Nour, O. Seitz, Y. Chabal, K. J. Balkus, *ACS Catal.* **2012**, *2*, 949.
[39] O. Akhavan, E. Ghaderi, *J. Phys. Chem. C* **2009**, *113*, 20214.
[40] Q. J. Xiang, J. G. Yu, M. Jaroniec, *Nanoscale* **2011**, *3*, 3670.
[41] J. G. Yu, J. Jin, B. Cheng, M. Jaroniec, *J. Mater. Chem. A* **2014**, *2*, 3407.
[42] Y. H. Ng, A. Iwase, A. Kudo, R. Amal, *J. Phys. Chem. Lett.* **2010**, *1*, 2607.
[43] W. G. Tu, Y. Zhou, Z. G. Zou, *Adv. Funct. Mater.* **2013**, *23*, 4996.
[44] F. Fresno, R. Portela, S. Suarez, J. M. Coronado, *J. Mater. Chem. A* **2014**, *2*, 2863.
[45] Y. Izumi, *Coord. Chem. Rev.* **2013**, *257*, 171.
[46] J. G. Yu, J. X. Low, W. Xiao, P. Zhou, M. Jaroniec, *J. Am. Chem. Soc.* **2014**, *136*, 8839.
[47] L. L. Tan, W. J. Ong, S. P. Chai, A. R. Mohamed, *Nanoscale Res. Lett.* **2013**, *8*, 465.
[48] W. J. Ong, M. M. Gui, S. P. Chai, A. R. Mohamed, *RSC Adv.* **2013**, *3*, 4505.
[49] Y. T. Liang, B. K. Vijayan, K. A. Gray, M. C. Hersam, *Nano Lett.* **2011**, *11*, 2865.
[50] Y. T. Liang, B. K. Vijayan, O. Lyandres, K. A. Gray, M. C. Hersam, *J. Phys. Chem. Lett.* **2012**, *3*, 1760.
[51] W. G. Tu, Y. Zhou, Q. Liu, Z. P. Tian, J. Gao, X. Y. Chen, H. T. Zhang, J. G. Liu, Z. G. Zou, *Adv. Funct. Mater.* **2012**, *22*, 1215.
[52] W. G. Tu, Y. Zhou, Q. Liu, S. C. Yan, S. S. Bao, X. Y. Wang, M. Xiao, Z. G. Zou, *Adv. Funct. Mater.* **2013**, *23*, 1743.
[53] X. S. Li, Q. A. Wang, Y. B. Zhao, W. Wu, J. F. Chen, H. Meng, *J. Colloid Interface Sci.* **2013**, *411*, 69.
[54] P. Q. Wang, Y. Bai, P. Y. Luo, J. Y. Liu, *Catal. Commun.* **2013**, *38*, 82.
[55] X. J. Lv, W. F. Fu, C. Y. Hu, Y. Chen, W. B. Zhou, *RSC Adv.* **2013**, *3*, 1753.
[56] E. P. Gao, W. Z. Wang, M. Shang, J. H. Xu, *Phys. Chem. Chem. Phys.* **2011**, *13*, 2887.
[57] S. W. Liu, J. G. Yu, M. Jaroniec, *Chem. Mater.* **2011**, *23*, 4085.
[58] S. W. Liu, J. G. Yu, B. Cheng, M. Jaroniec, *Adv. Colloid Interface Sci.* **2012**, *173*, 35.
[59] J. Zhang, J. G. Yu, Y. M. Zhang, Q. Li, J. R. Gong, *Nano Lett.* **2011**, *11*, 4774.
[60] S. W. Cao, J. G. Yu, *J. Phys. Chem. Lett.* **2014**, *5*, 2101.

[61] J. Zhang, J. G. Yu, M. Jaroniec, J. R. Gong, *Nano Lett.* **2012**, *12*, 4584.
[62] S. R. Pendlebury, A. J. Cowan, M. Barroso, K. Sivula, J. Ye, M. Grätzel, D. R. Klug, J. Tang, J. R. Durrant, *Energy Environ. Sci.* **2012**, *5*, 6304.
[63] J. Cheng, M. Zhang, G. Wu, X. Wang, J. H. Zhou, K. F. Cen, *Environ. Sci. Technol.* **2014**, *48*, 7076.
[64] V. Tripkovic, M. Vanin, M. Karamad, M. E. Bjorketun, K. W. Jacobsen, K. S. Thygesen, J. Rossmeisl, *J. Phys. Chem. C* **2013**, *117*, 9187.
[65] R. K. Yadav, J. O. Baeg, G. H. Oh, N. J. Park, K. J. Kong, J. Kim, D. W. Hwang, S. K. Biswas, *J. Am. Chem. Soc.* **2012**, *134*, 11455.
[66] R. K. Yadav, J. O. Baeg, A. Kumar, K. J. Kong, G. H. Oh, N. J. Park, *J. Mater. Chem. A* **2014**, *2*, 5068.
[67] T. S. Wu, L. Y. Zou, D. X. Han, F. H. Li, Q. X. Zhang, L. Niu, *Green Chem.* **2014**, *16*, 2142.
[68] H. C. Hsu, I. Shown, H. Y. Wei, Y. C. Chang, H. Y. Du, Y. G. Lin, C. A. Tseng, C. H. Wang, L. C. Chen, Y. C. Lin, K. H. Chen, *Nanoscale* **2013**, *5*, 262.
[69] M. R. Hoffmann, S. T. Martin, W. Y. Choi, D. W. Bahnemann, *Chem. Rev.* **1995**, *95*, 69.
[70] Q. J. Xiang, B. Cheng, J. G. Yu, *Appl. Catal. B* **2013**, *138*, 299.
[71] D. Lang, Q. J. Xiang, G. H. Qiu, X. H. Feng, F. Liu, *Dalton Trans.* **2014**, *43*, 7245.
[72] Q. J. Xiang, J. G. Yu, M. Jaroniec, *J. Phys. Chem. C* **2011**, *115*, 7355.
[73] P. Zhou, J. G. Yu, M. Jaroniec, *Adv. Mater.* **2014**, *26*, 4920.
[74] P. V. Kamat, *J. Phys. Chem. Lett.* **2011**, *2*, 242.
[75] P. Cheng, Z. Yang, H. Wang, W. Cheng, M. X. Chen, W. F. Shangguan, G. F. Ding, *Int. J. Hydrogen Energy* **2012**, *37*, 2224.
[76] X. Y. Zhang, Y. J. Sun, X. L. Cui, Z. Y. Jiang, *Int. J. Hydrogen Energy* **2012**, *37*, 811.
[77] Z. Khan, T. R. Chetia, A. K. Vardhaman, D. Barpuzary, C. V. Sastri, M. Qureshi, *RSC Adv.* **2012**, *2*, 12122.
[78] J. G. Yu, L. F. Qi, M. Jaroniec, *J. Phys. Chem. C* **2010**, *114*, 13118.
[79] J. G. Yu, Y. Hai, M. Jaroniec, *J. Colloid Interface Sci.* **2011**, *357*, 223.
[80] J. G. Yu, W. G. Wang, B. Cheng, B. L. Su, *J. Phys. Chem. C* **2009**, *113*, 6743.
[81] J. G. Yu, J. Zhang, M. Jaroniec, *Green Chem.* **2010**, *12*, 1611.
[82] W. Q. Fan, Q. H. Lai, Q. H. Zhang, Y. Wang, *J. Phys. Chem. C* **2011**, *115*, 10694.
[83] N. Li, G. Liu, C. Zhen, F. Li, L. L. Zhang, H. M. Cheng, *Adv. Funct. Mater.* **2011**, *21*, 1717.
[84] Q. Li, B. D. Guo, J. G. Yu, J. R. Ran, B. H. Zhang, H. J. Yan, J. R. Gong, *J. Am. Chem. Soc.* **2011**, *133*, 10878.
[85] Q. Li, H. Meng, J. G. Yu, W. Xiao, Y. Q. Zheng, J. Wang, *Chem. Eur. J.* **2014**, *20*, 1176.
[86] X. Y. Zhang, H. P. Li, X. L. Cui, Y. H. Lin, *J. Mater. Chem.* **2010**, *20*, 2801.
[87] L. Jia, D. H. Wang, Y. X. Huang, A. W. Xu, H. Q. Yu, *J. Phys. Chem. C* **2011**, *115*, 11466.
[88] X. J. Lv, W. F. Fu, H. X. Chang, H. Zhang, J. S. Cheng, G. J. Zhang, Y. Song, C. Y. Hu, J. H. Li, *J. Mater. Chem.* **2012**, *22*, 1539.
[89] P. Gao, J. C. Liu, S. Lee, T. Zhang, D. D. Sun, *J. Mater. Chem.* **2012**, *22*, 2292.
[90] S. X. Min, G. X. Lu, *J. Phys. Chem. C* **2012**, *116*, 25415.
[91] J. J. Ding, W. H. Yan, W. Xie, S. Sun, J. Bao, C. Gao, *Nanoscale* **2014**, *6*, 2299.
[92] X. R. Cao, G. H. Tian, Y. J. Chen, J. Zhou, W. Zhou, C. G. Tian, H. G. Fu, *J. Mater. Chem. A* **2014**, *2*, 4366.
[93] Y. K. Kim, H. Park, *Appl. Catal. B* **2012**, *125*, 530.
[94] N. Zhang, Y. H. Zhang, X. Y. Pan, M. Q. Yang, Y. J. Xu, *J. Phys. Chem. C* **2012**, *116*, 18023.
[95] J. Zhang, W. T. Zhao, Y. Xu, H. L. Xu, B. Zhang, *Int. J. Hydrogen Energy* **2014**, *39*, 702.
[96] A. Mukherji, B. Seger, G. Q. Lu, L. Z. Wang, *ACS Nano* **2011**, *5*, 3483.
[97] S. X. Min, G. X. Lu, *Int. J. Hydrogen Energy* **2012**, *37*, 10564.
[98] S. X. Min, G. X. Lu, *J. Phys. Chem. C* **2011**, *115*, 13938.
[99] H. I. Kim, G. H. Moon, D. Monllor-Satoca, Y. Park, W. Choi, *J. Phys. Chem. C* **2012**, *116*, 1535.
[100] Z. H. Sun, J. J. Guo, S. M. Zhu, L. Mao, J. Ma, D. Zhang, *Nanoscale* **2014**, *6*, 2186.
[101] K. Sayama, R. Yoshida, H. Kusama, K. Okabe, Y. Abe, H. Arakawa, *Chem. Phys. Lett.* **1997**, *277*, 387.
[102] H. Kato, M. Hori, R. Konta, Y. Shimodaira, A. Kudo, *Chem. Lett.* **2004**, *33*, 1348.
[103] K. Maeda, *ACS Catal.* **2013**, *3*, 1486.
[104] A. Iwase, Y. H. Ng, Y. Ishiguro, A. Kudo, R. Amal, *J. Am. Chem. Soc.* **2011**, *133*, 11054.
[105] Y. Sasaki, H. Nemoto, K. Saito, A. Kudo, *J. Phys. Chem. C* **2009**, *113*, 17536.
[106] X. W. Wang, G. Liu, Z. G. Chen, F. Li, L. Z. Wang, G. Q. Lu, H. M. Cheng, *Chem. Commun.* **2009**, 3452.
[107] T. Y. Peng, K. Li, P. Zeng, Q. G. Zhang, X. G. Zhang, *J. Phys. Chem. C* **2012**, *116*, 22720.
[108] P. Zeng, Q. G. Zhang, T. Y. Peng, X. H. Zhang, *Phys. Chem. Chem. Phys.* **2011**, *13*, 21496.
[109] M. Q. Yang, Y. H. Zhang, N. Zhang, Z. R. Tang, Y. J. Xu, *Sci. Rep.* **2013**, *3*, 3314.
[110] C. Lavorato, A. Primo, R. Molinari, H. Garcia, *ACS Catal.* **2014**, *4*, 497.
[111] H. I. Kim, S. Kim, J. K. Kang, W. Choi, *J. Catal.* **2014**, *309*, 49.
[112] P. Gao, D. D. Sun, *Appl. Catal. B* **2014**, *147*, 888.
[113] P. D. Tran, S. K. Batabyal, S. S. Pramana, J. Barber, L. H. Wong, S. C. J. Loo, *Nanoscale* **2012**, *4*, 3875.
[114] J. C. Liu, H. W. Bai, Y. J. Wang, Z. Y. Liu, X. W. Zhang, D. D. Sun, *Adv. Funct. Mater.* **2010**, *20*, 4175.
[115] J. Hong, K. Char, B. S. Kim, *J. Phys. Chem. Lett.* **2010**, *1*, 3442.
[116] J. S. Lee, K. H. You, C. B. Park, *Adv. Mater.* **2012**, *24*, 1084.
[117] H. F. Dang, X. F. Dong, Y. C. Dong, J. S. Huang, *Int. J. Hydrogen Energy* **2013**, *38*, 9178.
[118] X. K. Kong, C. L. Chen, Q. W. Chen, *Chem. Soc. Rev.* **2014**, *43*, 2841.
[119] S. P. Lonkar, A. A. Abdala, *J. Thermodyn. Catal.* **2014**, *5*, 132.
[120] M. Pumera, *Energy Environ. Sci.* **2011**, *4*, 668.
[121] P. Song, X. Y. Zhang, M. X. Sun, X. L. Cui, Y. H. Lin, *Nanoscale* **2012**, *4*, 1800.
[122] P. Zeng, Q. G. Zhang, X. G. Zhang, T. Y. Peng, *J. Alloys Compd.* **2012**, *516*, 85.
[123] Y. G. Lin, C. K. Lin, J. T. Miller, Y. K. Hsu, Y. C. Chen, L. C. Chen, K. H. Chen, *RSC Adv.* **2012**, *2*, 11258.
[124] C. H. Kim, B. H. Kim, K. S. Yang, *Carbon* **2012**, *50*, 2472.
[125] X. J. Bai, L. Wang, Y. F. Zhu, *ACS Catal.* **2012**, *2*, 2769.
[126] Y. H. Zhang, N. Zhang, Z. R. Tang, Y. J. Xu, *ACS Nano* **2012**, *6*, 9777.
[127] A. J. Du, S. Sanvito, Z. Li, D. W. Wang, Y. Jiao, T. Liao, Q. Sun, Y. H. Ng, Z. H. Zhu, R. Amal, S. C. Smith, *J. Am. Chem. Soc.* **2012**, *134*, 4393.
[128] H. Li, Z. Xia, J. Chen, L. Lei, J. Xing, *Appl. Catal. B* **2015**, *168–169*, 105.
[129] M. Q. Yang, Y. J. Xu, *J. Phys. Chem. C* **2013**, *117*, 21724.
[130] R. Long, N. J. English, O. V. Prezhdo, *J. Am. Chem. Soc.* **2012**, *134*, 14238.
[131] L. Zhang, Z. H. Xi, M. Y. Xing, J. L. Zhang, *Int. J. Hydrogen Energy* **2013**, *38*, 9169.
[132] X. J. Lv, S. X. Zhou, C. Zhang, H. X. Chang, Y. Chen, W. F. Fu, *J. Mater. Chem.* **2012**, *22*, 18542.
[133] B. L. Zhu, B. Z. Lin, Y. Zhou, P. Sun, Q. R. Yao, Y. L. Chen, B. F. Gao, *J. Mater. Chem. A* **2014**, *2*, 3819.

[134] J. G. Hou, Z. Wang, W. B. Kan, S. Q. Jiao, H. M. Zhu, R. V. Kumar, *J. Mater. Chem.* **2012**, *22*, 7291.
[135] X. W. Wang, L. C. Yin, G. Liu, *Chem. Commun.* **2014**, *50*, 3460.
[136] K. Chang, Z. W. Mei, T. Wang, Q. Kang, S. X. Ouyang, J. H. Ye, *ACS Nano* **2014**, *8*, 7078.
[137] T. T. Jia, A. Kolpin, C. S. Ma, R. C. T. Chan, W. M. Kwok, S. C. E. Tsang, *Chem. Commun.* **2014**, *50*, 1185.
[138] Y. Hou, Z. H. Wen, S. M. Cui, X. R. Guo, J. H. Chen, *Adv. Mater.* **2013**, *25*, 6291.
[139] J. Zhang, L. F. Qi, J. Ran, J. G. Yu, S. Z. Qiao, *Adv. Energy Mater.* **2014**, *4*, 1301925.
[140] Y. S. Chen, J. C. Crittenden, S. Hackney, L. Sutter, D. W. Hand, *Environ. Sci. Technol.* **2005**, *39*, 1201.
[141] J. G. Yu, W. G. Wang, B. Cheng, *Chem. Asian J.* **2010**, *5*, 2499.
[142] C. Chen, W. M. Cai, M. C. Long, B. X. Zhou, Y. H. Wu, D. Y. Wu, Y. J. Feng, *ACS Nano* **2010**, *4*, 6425.
[143] T. F. Yeh, C. Y. Teng, S. J. Chen, H. S. Teng, *Adv. Mater.* **2014**, *26*, 3297.
[144] F. K. Meng, J. T. Li, S. K. Cushing, M. J. Zhi, N. Q. Wu, *J. Am. Chem. Soc.* **2013**, *135*, 10286.
[145] Y. Z. Chen, C. Y. Zhang, X. J. Zhang, X. M. Ou, X. H. Zhang, *Chem. Commun.* **2013**, *49*, 9200.
[146] T. F. Yeh, F. F. Chan, C. T. Hsieh, H. S. Teng, *J. Phys. Chem. C* **2011**, *115*, 22587.
[147] J. X. Low, S. W. Cao, J. G. Yu, S. Wageh, *Chem. Commun.* **2014**, *50*, 10768.

Received: November 15, 2014
Published online: June 16, 2015